DOI: 10.1143/JPSJ.81.014707

Charge Distribution in the Surface BEDT-TTF Layer of α-(BEDT-TTF)$_2$I$_3$ at Room Temperature with Scanning Tunneling Microscopy

Eiichi MORI, Hidemasa USUI, Hirokazu SAKAMOTO, Kenji MIZOGUCHI*, and Toshio NAITO[1]

Department of Physics, Tokyo Metropolitan University, Hachioji, Tokyo 192-0397, Japan
[1]*Division of Chemistry and Biology, Graduate School of Science and Engineering, Ehime University, Matsuyama 790-8577, Japan*

(Received October 28, 2010; revised October 4, 2011; accepted October 24, 2011; published online December 16, 2011)

The charge distribution in the surface BEDT-TTF layer of the α-(BEDT-TTF)$_2$I$_3$ crystal with the charge disproportionation state at room temperature was studied in detail by a scanning tunneling microscope (STM), where BEDT-TTF (abbreviated as ET) is bis(ethylenedithio)tetrathiafulvalene. The obtained molecular charge distribution in the surface ET layer suggests that the electronic states of the surface ET layer at room temperature is the charge-ordered state, stable below 135 K in bulk crystals, rather than the charge disproportionation state above 135 K. The most probable mechanism underlying this remarkable finding is the particular freedom to the surface ET layer. The missing of the I_3 layer partially removes the structural constraint of the steric interaction between the thermally vibrating ethylene groups and the neighboring two I_3 layers. This mechanism would have something in common with the layered ET complexes.

KEYWORDS: charge transfer salt, charge ordering, charge disproportionation, surface electronic states, STM

1. Introduction

Recently, charge ordering (CO) and charge disproportionation (CD) in strongly correlated organic systems, where the intersite Coulomb interaction V is large enough, have attracted much interest. The number of π charges on the molecules in a unit cell could be nonequivalent in the CO and CD states. The CO state represents the long-range ordering of the intermolecular charge distribution caused by the intersite Coulomb repulsion V with the insulating electronic states, which is similar to the charge density wave in phenomenon, but not in mechanism. However, the CD state is similar to the CO state, but is caused by anisotropic transfer integrals in the unit cell, which might be metallic in the electronic states. It has been reported that α-(BEDT-TTF)$_2$I$_3$ shows both the CD and CO states in different temperature ranges,[1–3] where BEDT-TTF (abbreviated as ET, hereafter) is bis(ethylenedithio)tetrathiafulvalene. This system has currently attracted huge interest as the typical bulk example of the massless Dirac fermion system[2,3] along with the layer graphene system.[4]

The a–b plane projection of the crystal structure of α-(ET)$_2$I$_3$ determined by X-ray analysis[5,6] is shown in Fig. 1, which contains four nonequivalent ET molecules, i.e., A, A′, B, and C. On the distribution of the molecular charges in the unit cell, there are three independent sites in the CD state at room temperature (RT), but roughly two in the CO state below $T_C = 135$ K. It is confirmed that the intermolecular charge distribution below T_C shows a horizontal stripe pattern with rich charges of 0.7–0.8 at the A and B sites and poor charges of 0.2–0.3 at the A′ and C sites,[5] which is consistent with the results of NMR analysis,[7] Raman study,[8] and theoretical prediction.[9] The horizontal stripe means that the ordered direction of charge-rich or charge-poor molecules is perpendicular to the molecular stacking a-axis. Above the transition temperature, this system behaves as a semi-metal with weak charge disproportionation.

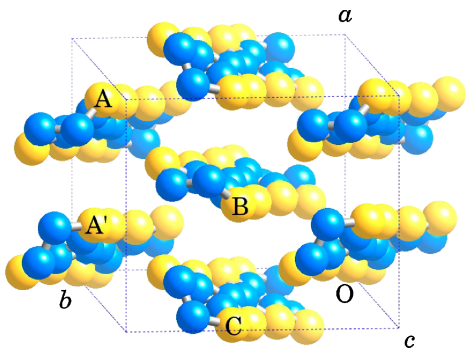

Fig. 1. (Color online) Structure of α-(BEDT-TTF)$_2$I$_3$ determined by X-ray analysis at 300 K.[5,6] The a–b plane is parallel to the observed surface. Hydrogen atoms are not indicated. The labels A, A′, B, and C are the same as those reported in ref. 5. $a = 0.9187$ nm, $b = 1.0793$ nm, $c = 1.7400$ nm, $\alpha = 96.957°$, $\beta = 97.911°$, and $\gamma = 90.795°$.

Surface molecular charges have been studied in several molecular crystal systems. In an earlier study of the present system α-(ET)$_2$I$_3$, scanning tunneling microscopy (STM) images were assigned to the proton 1s orbitals at the end ethylene.[10] π electrons were, however, present on sulfur atoms, but absent not only on these protons but also on ethylene carbons, as demonstrated by the molecular orbital calculation for the highest occupied molecular orbital (HOMO) of ET molecule in Fig. 2. Thus, further investigation of the molecular charge distribution in α-(ET)$_2$I$_3$ is needed. Yoshimura *et al.* have reported the surface superstructure of ET molecules in the observed b–c plane parallel to the I_3 layers in β-(ET)$_2$I$_3$.[11] They observed a periodic structural modulation consisting of two alternative different spacings of 0.84 and 0.68 nm along the c-axis with $c = 0.66$ nm in the bulk crystal. Thus, it is very interesting to investigate the surface structure of the present system α-(ET)$_2$I$_3$ with the same composition as but a different structure from β-(ET)$_2$I$_3$. Ishida and coworkers have reported the surface reconstruction at various temperatures in the quasi-one-dimensional system β-(ET)$_2$PF$_6$ with the

*E-mail: mizoguchi@phys.se.tmu.ac.jp

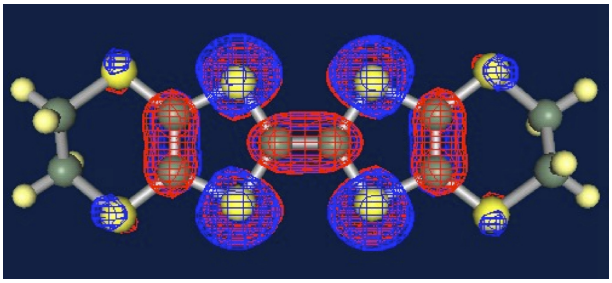

Fig. 2. (Color online) Molecular structure of BEDT-TTF with HOMO molecular orbitals calculated by MOPAC. The size of the orbitals represents the relative fraction of HOMO electrons.

CO ground state.[12–14] They reported the remarkable surface reconstruction along the *b*-direction perpendicular to the observed *a*–*c* plane at RT, which reaches up to 0.15 nm following their analysis based on the assumption for the surface reconstruction solely to be structural, but not the redistribution of charges. However, note that Nogami and Mori have reported a CO ground state with a large charge distribution from 0 to +0.8 electrons on the four ET molecules in the unit cell at 90 K in this system.[14] Thus, it is also interesting to study the origin of the surface reconstruction of the present system α-$(ET)_2I_3$ in detail, as one of the organic molecular systems. In θ-$(ET)_2RbZn(SCN)_4$, Yoneyama and coworkers reported the electronic states at RT with STM.[15] It has been considered that the metallic state at RT transforms into the CO insulator below 190 K.[16] However, Yoneyama *et al.* discovered the brightness pattern corresponding to the charge distribution among the molecules in the unit cell and proposed a vertical-stripe-type CO state at RT. This finding raises a possibility that the electronic states of the surface layer are independent of those of bulk crystals in organic molecular systems. Thus, it is important to clarify whether it is a special example or a universal feature of organic layered crystals.

In this research, we study the CD state of α-$(ET)_2I_3$ at RT by STM. On the basis of the hydrogen-like 3*p* orbitals at the end sulfur atoms in each molecule, the observed topographies are analyzed in detail, which show a small but distinct deviation from the reported crystal structure and molecular charges. Two possible origins of the deviation are discussed in detail, on the basis of the results of the electric field analysis of an I_3^- layer. Finally, we conclude that the CD state is not found, but that the CO state is observed in the surface ET layer even at RT. We also propose a model for interpreting this interesting finding, similar to that in the θ-$(ET)_2RbZn(SCN)_4$ case.

2. Experimental

STM was carried out at RT with easyScan 2, manufactured by NanoSurf®, with a mechanically sharpened $Pt_{0.8}Ir_{0.2}$ wire. Throughout this study, the tunneling current and tip potential were set to 1 nA and 10 mV, respectively. Single crystals of α-$(ET)_2I_3$ were prepared following a previously reported procedure[17] with chlorobenzene instead of tetrahydrofuran as the solvent. The typical crystal dimensions were $5 \times 2 \times 0.05\,mm^3$. The instrumental drift of STM was eliminated on the basis of the reported lattice parameters[5] with the SPIP™ image processing software.

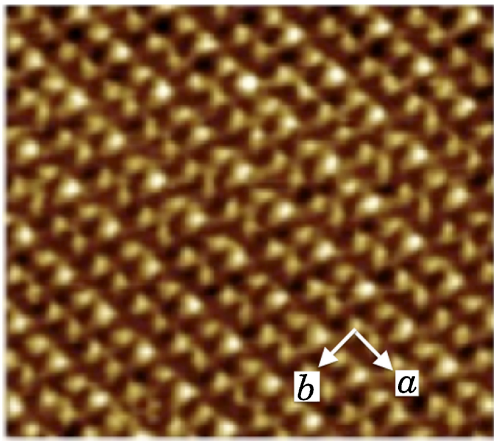

Fig. 3. (Color online) STM image of α-$(BEDT\text{-}TTF)_2I_3$ in $\approx 7.0 \times 6.5\,nm^2$, where the thermal drift was corrected with the reported lattice parameters.[5] The assigned *a*- and *b*-axes are indicated by the arrows.

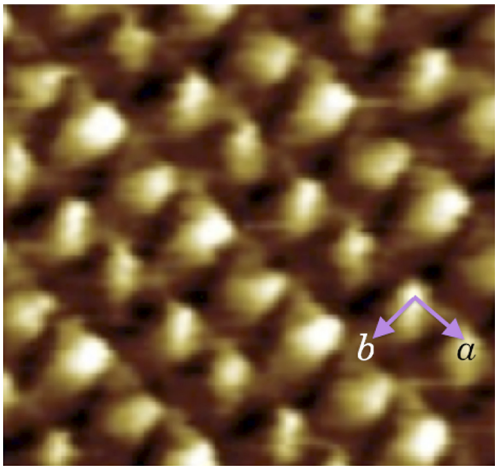

Fig. 4. (Color online) Enlarged STM image of α-$(BEDT\text{-}TTF)_2I_3$ at $\approx 2.8 \times 2.6\,nm^2$. The brightest area in each unit cell is assigned to ET(B).

3. Discussion

3.1 *STM images of α-(BEDT-TTF)$_2I_3$*

Figure 3 demonstrates the *a*–*b* surface-scan image of α-$(ET)_2I_3$ at over $\approx 7.0 \times 6.5\,nm^2$. The scanned image in the narrow area of $\approx 2.8 \times 2.6\,nm^2$ is shown in Fig. 4. We notice the following two points from these images. One is the absence of a noticeable long-range modulation. The other is the definite periodic structure made of four types of bright areas with characteristic features in brightness and shapes, which is helpful as the tool for assignment. The molecular stacking *a*-axis along the A–A′ and B–C molecular arrays is easily assigned to run from the top left to the bottom right. The brightest areas can be reasonably assigned to the B site [hereafter, represented as ET(B)] in Fig. 1, because the molecular charge in the B site is largest at RT.[5] Thus, less bright areas in the B–C arrays, which contain the brightest ET(B), are assigned to the C site [ET(C)]. Arrays with small and less bright areas in between the B–C arrays correspond to the A and A′ [ET(A) and ET(A′)] arrays, which are equivalent to each other at RT within the experimental

Table I. Tip height difference Δh_i measured by STM topography relative to ET(B) from Figs. 4 and 9 for α-(BEDT-TTF)$_2$I$_3$. $h_{m,i}$ is estimated from the simulation of the topographies and is utilized to estimate $\Delta_{\delta,i}$. $\Delta_{S,i}$ is the relative height difference of the relevant sulfur atom to ET(B) measured from the a–b plane, extracted from the structural data.[5,6] δ_i represents the angle of 3p orbital axis against the a–b plane and $\Delta_{\delta,i}$ is the relative height change caused by δ_i, which is proportional to $h_{m,i}$. Δ_{CD_i} is the expected tip height due to the charge distribution caused by the CD state at RT and $\Delta h_{ap,i} = \Delta h_i - \Delta_{S,i} - \Delta_{\delta,i} - \Delta_{CD_i}$ is the apparent change caused by the surface reconstruction over the CD state in case (a). $\Delta h_{m,i} = \Delta h_i - \Delta_{S,i} - \Delta_{\delta,i}$ is the experimental relative height in case (b), which gives the ratio of molecular charge with respect to ET(B), i.e., ρ_i/ρ_B. All the length scales are in nm.

	Δh_i	$h_{m,i}$	$\Delta_{S,i}$	δ_i (deg)	$\Delta_{\delta,i}$	Case (a)		Case (b)	
						Δ_{CD_i}	$\Delta h_{ap,i}$	$\Delta h_{m,i}$	ρ_i/ρ_B
B	0	0.23	0	10.4	0	0	0	0	1
C	−0.025(7)	0.21	−0.003	12.9	−0.003	−0.007	−0.012	−0.019	0.36
A	−0.012(7)	0.22	0.000	11.3	−0.003	−0.003	−0.006	−0.009	0.61
A′	−0.022(7)	0.21	−0.002	11.2	−0.002	−0.003	−0.015	−0.018	0.38

Table II. Relative molecular charge $\rho_i/\sum_i \rho_i$ for α-(BEDT-TTF)$_2$I$_3$ in case (b), which is compared with that estimated by X-ray analysis.[5] Note the broken inversion symmetry between ET(A) and ET(A′), which suggests the rich charge stripes of the B–A–B type. The parentheses show uncertainty in the last digit.

Site	Present results	X-ray results	
	RT	RT	20 K
B	0.42(8)	0.29(2)	0.35(4)
C	0.16(2)	0.21(3)	0.12(5)
A	0.26(5)	0.25(2)	0.39(5)
A′	0.16(2)	0.25(2)	0.14(5)

uncertainty, following the reported molecular structure and charges, as shown by $\Delta_{S,i}$ and δ_i in Table I and by the X-ray results at RT in Table II.[5] Figure 2 shows the molecular HOMO orbitals of an ET molecule, which will be observed with an STM probe tip. Since the atoms of end ethylenes have no HOMO orbitals, one should probe one of the four end sulfur 3p orbitals in the a–b plane with STM. Thus, the interpretation of the STM image in terms of the proton atoms of the end ethylene in ref. 10 needs to be reexamined. The symmetry axes of the sulfur 3p orbitals in both ends tilted slightly from the normal to the molecular plane because of the twisted ethylene sp^3 bondings. However, it is safely assumed that one observes the time-averaged direction of the symmetry axis for the 3p orbital in STM, that is, the normal to the molecular plane because of the rapid thermal motion between the bistable twisted positions.

The structure determined by X-ray analysis[5] is superposed on the STM image in Fig. 5. The bright areas show a reasonable agreement with the 3p orbitals of sulfur atoms in the position and direction without sizable reconstructions within the limited accuracy of the wavefunction image. Here, it is assumed that the bright areas are assigned to the halves of the sulfur 3p orbitals on the single side of the molecular plane, because the symmetry axis of the sulfur 3p orbital tilts by about 12° out of the a–b plane. The present assignment of the molecular sites is also consistent with the characteristic feature of the X-ray structure; one can see a weak dimerization along the A–A′ array corresponding to

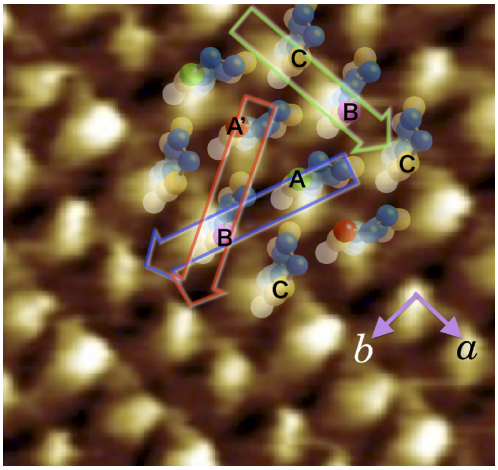

Fig. 5. (Color online) Crystal structure assigned to the STM image of α-(BEDT-TTF)$_2$I$_3$, with which the topographies in Fig. 9 are simulated. The balls with A′ [ET(A′)], A [ET(A)], B [ET(B)], and C [ET(C)] represent the relevant sulfur atoms. This model assignment corresponds to the a–b plane observed from the reverse side of Fig. 1. The three large arrows represent the direction of the topography shown in Fig. 9.

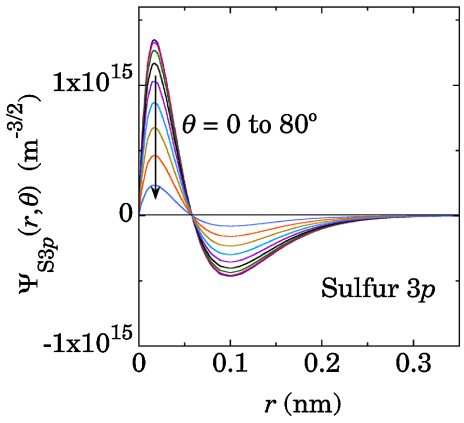

Fig. 6. (Color online) 3p wavefunction of a sulfur atom with the effective nuclear charge of $Z_{eff} = 5.48$ for every 10° of θ from 0 to 80°, which is defined in Fig. 7. r is the distance from the sulfur nucleus. STM observes the region further than $r \approx 0.1$ nm in α-(BEDT-TTF)$_2$I$_3$.

the alternating transfer integrals of a2 and a3 in the same notification as that in ref. 5.

3.2 *Analysis of STM topography*

The wavefunction Ψ^i_{S3p} for the 3p orbital of the relevant sulfur atom in the ET(i) molecule (i = B, C, A, or A′) is expressed as

$$\Psi^i_{S3p} = \sqrt{\rho_i f_S}\,\Psi_{S3p}, \tag{1}$$

where ρ_i is the molecular charge number in the HOMO band of each ET(i), f_S is the fraction of 3p charge at the sulfur atom in each ET(i), and Ψ_{S3p}, as shown in Fig. 6, is the wavefunction of the sulfur 3p orbital with the atomic number $Z = 16$, expressed as

$$\Psi_{S3p} = \sqrt{\frac{2}{\pi}\left(\frac{Z_{eff}}{a_0}\right)^5}\,\frac{r}{81}\left(6 - \frac{Z_{eff}r}{a_0}\right)\exp\left(-\frac{Z_{eff}r}{3a_0}\right)\cos\theta, \tag{2}$$

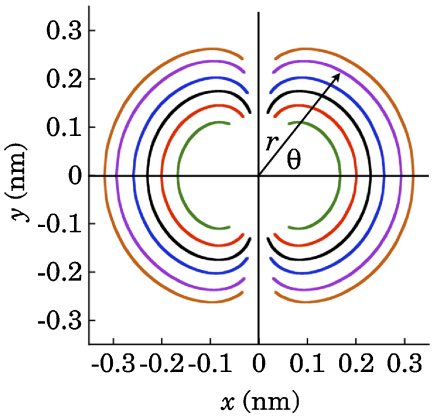

Fig. 7. (Color online) Constant amplitude contour of $3p$ wavefunction of sulfur atom deduced from Fig. 6 for the STM topography analysis in α-(BEDT-TTF)$_2$I$_3$. The abscissa corresponds to the symmetry axis of the $3p$ orbital of a sulfur atom at the origin, perpendicular to the molecular plane corresponding to the vertical line. Each constant amplitude of $|\Psi_{S3p}|$ is 5×10^{12}, 1×10^{13}, 2.5×10^{13}, 5×10^{13}, 1×10^{14}, and 2×10^{14} m$^{-3/2}$ from the outer to the inner.

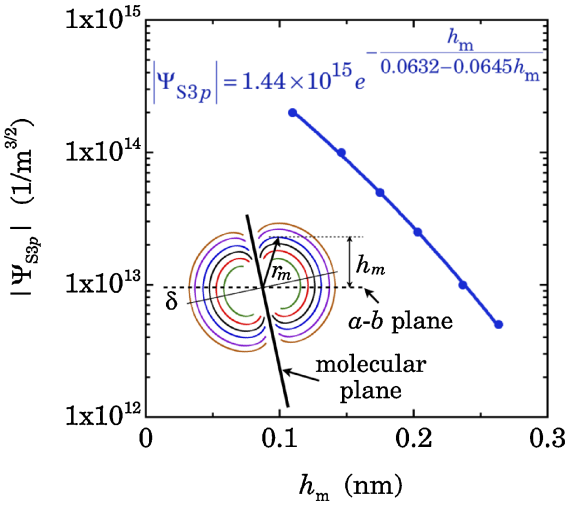

Fig. 8. (Color online) Maximum height h_m estimated from each Ψ_{S3p} wavefunction contour in the inset, where the symmetry axis (thin solid line) of the $3p$ wavefunction tilts by $\delta \approx 12^\circ$ against the a–b plane described by the dashed horizontal line through the sulfur atom. The analytical expression approximately describes $|\Psi_{S3p}|$ as a function of h_m, which is applicable to the STM topography analysis in the a–b plane of α-(BEDT-TTF)$_2$I$_3$.

where $a_0 = 5.29 \times 10^{-11}$ m is the Bohr radius and $Z_{\rm eff} = 5.48$ is the effective nuclear charge for the sulfur atom, in which the screening effect of the inner core electrons is taken into account.[18] The representative contour of the constant Ψ_{S3p} is shown in Fig. 7. The tunnel current I in the limits of small voltage and low temperature is expressed as[19]

$$I_{\rm tunnel} = \left(\frac{2\pi}{\hbar}\right) e^2 V_{\rm a} \Sigma_i |M_{\mu,i}|^2 \delta(E_i - E_{\rm F}) \delta(E_\mu - E_{\rm F}), \quad (3)$$

where $V_{\rm a}$ is the applied voltage, $M_{\mu,i}$ is the tunneling matrix element between the states Ψ_μ of the probe tip and Ψ^i_{S3p} of the relevant sulfur atom, and E_i, E_μ, and $E_{\rm F}$ are the energies of the states Ψ^i_{S3p} and Ψ_μ in the absence of tunneling, and the Fermi energy of the tip, respectively. The expected change in the probe height in the topography of the constant-current mode would be caused by the matrix element expressed as

$$M_{\mu,i} = -\left(\frac{\hbar^2}{2m}\right) \int {\rm d}S \cdot (\Psi^*_\mu \nabla \Psi^i_{S3p} - \Psi^i_{S3p} \nabla \Psi^*_\mu), \quad (4)$$

where the integral is over any surface lying entirely within the barrier region. Here, the probe wavefunction Ψ_μ is safely assumed to be independent of ET(i), and thus, the difference in Ψ^i_{S3p} in the constant-current mode produces the observed change in the probe height Δh. If the molecular charge on each ET(i) is not uniform in the unit cell, as in the CD state at RT in α-(ET)$_2$I$_3$, the tip height depends on the local density of states proportional to $\rho_i f_{\rm S}$ under the constant-tunneling-current condition.

Thus, the condition for providing the same tip current at the local coordinates $\mathbf{r}_i$ for the end sulfur atom of ET(i) and $\mathbf{r}_j$ for ET(j) is expressed as

$$\Psi^i_{S3p}(\mathbf{r}_i) = \Psi^j_{S3p}(\mathbf{r}_j),$$
$$\frac{\Psi^i_{S3p}(\mathbf{r}_i)}{\Psi^j_{S3p}(\mathbf{r}_j)} = \sqrt{\frac{\rho_i}{\rho_j}} \frac{\Psi_{S3p}(\mathbf{r}_i)}{\Psi_{S3p}(\mathbf{r}_j)} = 1, \quad (5)$$

assuming that $f_{\rm S}$ is independent of the site. Thus, the ratio of the charge number in ET(i) to ET(j) can be described in terms of the amplitude of Ψ_{S3p} as

$$\frac{\rho_i}{\rho_j} = \left[\frac{\Psi_{S3p}(\mathbf{r}_j)}{\Psi_{S3p}(\mathbf{r}_i)}\right]^2. \quad (6)$$

Figure 8 shows a more realistic configuration with a tilting angle of 12° for $\Psi_{S3p}(h_{\rm m})$ in α-(ET)$_2$I$_3$, where $h_{\rm m}$ is the maximum height of the relevant contour curve, as shown in the inset. Since $\Psi_{S3p}(h_{\rm m})$ decays exponentially, the following phenomenological formula is derived to reproduce the data:

$$|\Psi_{S3p}| = a \exp\left(-\frac{h_{\rm m}}{h_0}\right) = a \exp\left(-\frac{h_{\rm m}}{b - c h_{\rm m}}\right). \quad (7)$$

As shown in Fig. 8, the data points around $h_{\rm m} \approx 0.2$ nm can be reproduced well with the parameters $a = 1.44 \times 10^{15}$ m$^{-3/2}$, and the correlation length $h_0 = b - c h_{\rm m}$ nm, where $b = 0.0632$ nm and $c = 0.0645$. With this relation, the ratio of the molecular charge for ET(i) against ET(B) in terms of Ψ_{S3p}, as shown in eq. (6), can be expressed with the relative topographic difference $\Delta h_{{\rm m},i}$ as

$$\frac{\rho_i}{\rho_{\rm B}} = \left[\frac{\Psi_{S3p}(h_{\rm m,B})}{\Psi_{S3p}(h_{\rm m,B} + \Delta h_{{\rm m},i})}\right]^2$$
$$= \exp\left\{-2\left[\frac{h_{\rm m,B}}{b - c h_{\rm m,B}} - \frac{h_{\rm m,B} + \Delta h_{{\rm m},i}}{b - c(h_{\rm m,B} + \Delta h_{{\rm m},i})}\right]\right\}, \quad (8)$$

where $h_{\rm m,B}$ is the maximum height for ET(B) and $h_{{\rm m},i} = h_{\rm m,B} + \Delta h_{{\rm m},i}$ for ET(i). $\Delta h_{{\rm m},i}$ can be directly measured as Δh_i for each ET(i); the tip height difference from ET(B) with some corrections is described in Table I.

3.3 *Simulation of topography*

In Fig. 9, the superposed topographies along the directions of large arrows in Fig. 5 are shown with the solid curves, which enables us to average the random error out graphically to estimate the probe height change Δh_i for each ET(i) against ET(B). The characteristic features of the topographies are as follows.

- The height at ET(A′) is almost of the same magnitude as that at ET(C), and the height at ET(A) appears in

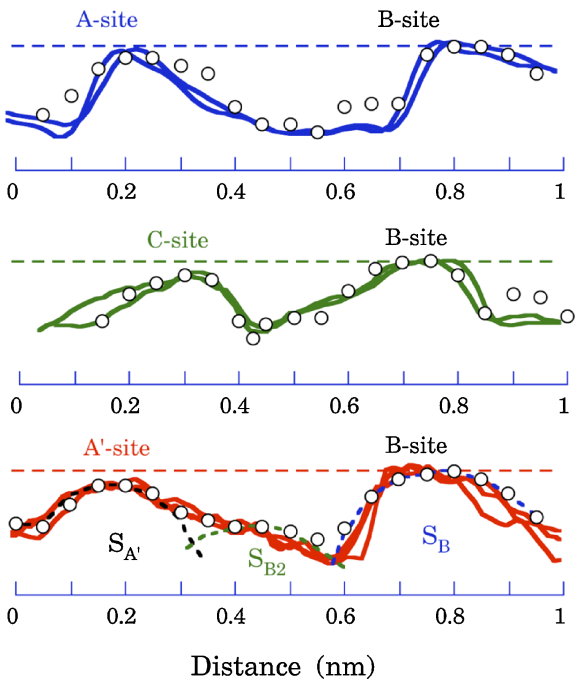

Fig. 9. (Color online) STM topographies of α-(BEDT-TTF)$_2$I$_3$ (solid curves) and the simulations (open circles) with $\Sigma_i|\Psi^i_{S3p}|^2$, where the molecular charge ratio ρ_i/ρ_B in Table I was taken into account. The topographies were measured along the arrows in Fig. 5. The horizontal dashed straight lines are visual guides at the top of the S_B site. The broken curves for the bottom A′–B scan show individual contributions of each sulfur atom at S_B and S'_A, and S_{B2}. From S_B, note that S_{B2} is 0.1 nm inside. The vertical scale is the same as the horizontal one.

between ET(B) and ET(A′) or ET(C). This observation suggests the symmetry breaking in the surface ET layer between ET(A) and ET(A′). Note that $\Delta_{S,i}$ and δ_i in ET(A) and ET(A′) are almost equivalent to each other in the bulk system at RT, as shown in Table I.

- Both steep changes and long tails are found.

Concerning the first point, there are several possibilities of providing particular surface states different from those in the bulk crystal case:

(1) the molecular reconstruction [case (a)]; the displacement along the c^* direction and the rotation of the symmetry axis of $3p$ orbital out of the crystal plane, etc.,
(2) molecular charge redistribution in the unit cell [case (b)],
(3) both cases (a) and (b) contribute to the observed result [case (c)].

It is good to recognize how these parameters change across the phase transition at 135 K from the CD state to the CO state. A remarkable molecular charge redistribution has occurred across the phase transition from nearly equivalent charges within the unit cell at RT, as shown in Table II. In contrast, the displacement along the c^*-direction is as small as 0.001 nm or less and the molecular rotation is as small as 0.75°, resulting in a 0.002 nm change in the relevant sulfur position along the c^* direction of α-(ET)$_2$I$_3$.[5)] Here, note that this displacement along the c^* direction is much less than the observed difference Δh_i, as shown in Table I. With the heights from each sulfur position, i.e., $h_{m,i} \approx 0.23 \pm 0.06$ nm for ET(B) and $\approx$ 0.21–0.22 nm for the other ET sites, and the reported structural data,[5,6)] the corrections $\Delta_{S,i}$ for the sulfur positions, $\Delta_{\delta,i}$ for the angle of $3p$ orbitals and Δ_{CD_i} for the charge distribution of the CD state at RT are estimated and shown in Table I.

First, let us consider case (a) under the assumption that the apparent relative heights $\Delta h_{ap,i}$ in Table I are totally dominated by the c^*-axis reconstruction of the surface layer molecules. In this case, one interesting point is that the tip position at the most positively charged ET(B) is highest in the unit cell. What governs the structural reconstruction normal to the a–b plane in the surface ET layer? The ET molecule in the surface layer interacts with

- neighboring ET molecules within the surface ET layer, and
- a neighboring I_3 layer and the interior sets of $ET_2 + I_3$ layers below the surface.

It is helpful to note that the ET–ET interaction within the ET layer governs the band structure of the π electron system, which is highly two-dimensional (2D) because of poor interlayer coupling by the separating anion layer. The binding energy of 2D π electrons is sufficiently large to keep the location of the sulfur atoms normal to the a–b plane almost unchanged even in the phase transition from the CD state at RT to the CO state below 135 K.[5)] In contrast, the Coulomb attraction toward the interior I_3 layer can be a major origin of the sizable structural reconstruction. Thus, we focus on the second point hereafter.

On the effects of the interior layers, it is good to separate the cases: (1) double layers comprising of an ET_2^+ layer and an I_3^- layer and (2) one I_3^- layer nearest to the surface ET_2^+ layer. Magonov *et al.* have reported that the STM or AFM tip occasionally removes surface molecules, but only as sets of ET_2 and I_3 molecules or layers in α-(ET)$_2$I$_3$, which suggests that the charge transfer from the ET_2^+ layers to the I_3^- layers strongly bounds each other, even in surface layers.[10)] Since a double layer produces an electric field only inside, the interior double layers do not affect the surface ET layer in the first-order approximation, as described in Fig. 10. Thus, the I_3^- layer, the interior neighbor of the surface ET layer, would play a crucial role in the structural surface reconstruction; the electric field of the I_3^- layer attracts positively charged ET molecules. As the second-order effect, the local structure of the electric field near the double layer couples the neighboring double layers together, which rapidly decays with increasing distance from the I_3^- layer. To estimate the force exerted on each ET molecule in the unit cell by the neighboring I_3^- layer, the potential produced by the I_3^- layer is estimated as a function of the distance from the I_3^- layer.

The electric field strength produced by the nearest I_3^- layer was estimated qualitatively under the assumption that the electron transferred from each set of two ET molecules to an I_3 molecule is located equally on both ends of the I_3^- molecule, that is, $I^{-1/2}$–I^0–$I^{-1/2}$. The potential profile within the central unit cell caused by 98 I_3^- ions in the 49 unit cells of the a–b plane is confirmed to be flat within ± 1 and $\pm 0.3\%$ in the plane at $0.2c = 0.34$ nm and in the center plane at $0.5c$ from the I_3^- layer, respectively. The electric field in the a–b plane derived from the potential profile shows the distribution of ± 6 and $\pm 1\%$ in the $0.3c = 0.52$ nm and center planes, respectively. Since the contour profile of

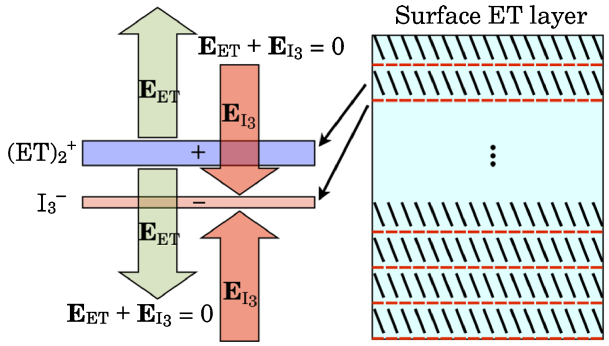

Fig. 10. (Color online) Schematic picture of the electric fields produced by a set of ET_2 and I_3 layers with the same charge density in α-(BEDT-TTF)$_2$I$_3$. The electric field produced by a double layer of $ET_2^+ + I_3^-$ is confined inside the double layer. That is, outside the double layer, the electric field cancels out. However, the electric field near the double layer is only partly cancelled, which binds the neighboring double layers. Thus, the surface ET layer approximately feels only the electric field of the nearest I_3^- layer.

the calculated potential and electric field shows a concentric profile, the origin of this distribution would be due to an edge effect caused by the finite number of I_3^- ions in the present calculation, on the basis of the Coulomb potential with a long-range nature proportional to the inverse of the distance. Thus, it is concluded that the approximately uniform electric field perpendicular to the *a*–*b* plane is produced by the I_3^- layer.

In a uniform electric field, ET molecules are pressed against the I_3^- layer in proportion to the charge number on each ET molecule. ET(B) has the largest charge number among the four nonequivalent ET molecules, which predicts the largest sink for ET(B) over the others, ET(A), ET(A′), and ET(C). This situation also holds for the molecular rotation as the reconstruction of the surface layer. The torque under the homogeneous $\mathbf{E}_{I_3}$ is directly proportional to the charge number of the molecule, which also leads us to expect the smallest tip height for ET(B). Thus, the absolute contradiction in these predictions with the observation of the largest, positive apparent tip height for ET(B) over the others suggests that the attractive Coulomb interaction between ET_2^+ and I_3^- layers is not the dominant factor for interpreting the surface height difference in α-(ET)$_2$I$_3$. Therefore, it is concluded that the crucial interaction responsible for the observed surface reconstruction is not the Coulomb attraction between the I_3^- layer and the ET_2^+ molecule, but some modification of the ET–ET interaction under special circumstances in the surface layer, which minimizes the total surface energy. It would be the structural freedom from the absence of the steric interaction between the rapidly vibrating end-ethylene group and the missing I_3 layer, which might cause small angle rotations of the molecular plane to realize the lowest surface energy state.

Next, we discuss the most probable case (b); the main mechanism of Δh_i is ascribed to the charge redistribution among the four nonequivalent ET molecules in the unit cell. In Fig. 9, the observed topographies (solid curves) are simulated using the calculated contour profile of $\Sigma_i|\Psi^i_{S3p}|^2$ for the tunneling current with open circles on the basis of case (b). Note that the characteristic structures of the topographies can be reproduced reasonably by the sulfur 3*p* wavefunctions. The steep changes near the sulfur atoms originate from the node of the 3*p* wavefunction, whereas the longer tails originate from the S3*p* wavefunctions of the neighboring sulfur atoms. In particular, the second sulfur atom below by 0.1 nm in ET(B) is essential to reproduce the topography along the A′–B direction.

The derived ratios of the molecular charges ρ_i/ρ_B in case (b) are presented in Table I. To make a comparison with the reported results[5] obtained using an empirical method,[20] the fraction of the molecular charge $\rho_i/\sum_i \rho_i$ is presented in Table II, along with the reported results both at RT and 20 K for the crystal α-(ET)$_2$I$_3$. The experimental equivalence of the charge number between ET(A) and ET(A′) in the CD state of the bulk at RT is completely missing in the surface layer. In contrast, the fraction in ET(A′) becomes equal to ET(C) within the uncertainty, similar to the CO state at 20 K in the bulk crystal. From these findings, it is strongly suggested that the CD state becomes unstable in the surface ET layer; in contrast, the charge redistributed state similar to the CO ground state below 135 K is stabilized. This remarkable difference from the bulk result can be induced by a small angle of molecular rotation, which can strongly modify the electronic states of the surface ET layer. Here, note again that the largest molecular rotation is only 0.75° in the CD-to-CO phase transition at 135 K.[5]

Thus, we propose that the possible reason for this charge redistribution in the surface ET layer is the absence of the constraint interaction between the thermally vibrating ethylene group of ET molecules and the missing second I_3^- neighboring layer. The ET–ET interaction without the constraint of the I_3 molecules would realize the most stable ground state of the CO state in α-(ET)$_2$I$_3$ even at RT. The present finding suggests that the large-amplitude, bistable thermal vibration of ethylene groups interferes with the ground state molecular conformation of the ET layer at RT in the α-(ET)$_2$I$_3$ crystals. The weakening of the thermal vibration at 135 K results in the phase transition from the metallic CD state at RT to the insulating CO state in α-(ET)$_2$I$_3$ crystals. This mechanism has something in common with the other organic layered systems with segregated structures, such as β-(ET)$_2$PF$_6$ and θ-(ET)$_2$RbZn(SCN)$_4$, which were mentioned in §1.

4. Conclusions

We have studied α-(ET)$_2$I$_3$ to directly observe the CD state at RT with STM, and found that the electronic states of the surface ET layer were not the CD state, but the CO state, in contrast to the bulk crystal result.[5] That is, the electronic states of the surface ET layer is independent of those of the bulk crystal because of the reduced constraint by the missing surface anion layer, which should have something in common with the other layered organic charge transfer salts.

On the basis of the hydrogen-like 3*p* orbitals at the end sulfurs in each ET molecule, the observed topographies can be reasonably reproduced with a small, but distinct deviation from those of the bulk crystals. The two mechanisms, i.e., (a) the structural reconstruction and (b) the molecular charge

redistribution in the surface layer, were examined by electric field analysis, which suggests that the molecular charge redistribution is the unique origin of the observed deviation. The estimated charge distribution in the surface ET layer is similar to the CO state of bulk α-$(ET)_2I_3$ crystal below T_C, but not to the CD state of the crystals at RT, shown by the broken symmetry between ET(A) and ET(A′) and the horizontal charge stripe of the B–A–B type, which are induced by the lack of constraint interaction layer. This understanding suggests that the phase transition at 135 K from the metallic CD state to the insulating CO state in the α-$(ET)_2I_3$ crystals is partly driven by the termination of the thermal bistable vibration in the end ethylene groups of ET molecules. This conclusion would provide important information to further advance the research on the electronic states of strongly correlated organic crystals.

Acknowledgments

One of the authors (KM) would like to express his sincere thanks to Professor Sawa for valuable data and discussions, and Dr. Shimoi and Dr. Iwano for helpful discussions. This work was partly supported by a Grant-in-Aid for Scientific Research on Priority Areas (17067015) from the Ministry of Education, Culture, Sports, Science and Technology and by a Grant-in-Aid for Scientific Research C (22540371) from the Japan Society for the Promotion of Science.

1) N. Tajima, M. Tamura, Y. Nishio, K. Kajita, and Y. Iye: J. Phys. Soc. Jpn. **69** (2000) 543.
2) N. Tajima and K. Kajita: Sci. Technol. Adv. Mater. **10** (2009) 024308.
3) A. Kobayashi, S. Katayama, and Y. Suzumura: Sci. Technol. Adv. Mater. **10** (2009) 024309.
4) G. Li, A. Luican, and E. Y. Andrei: Phys. Rev. Lett. **102** (2009) 176804.
5) T. Kakiuchi, Y. Wakabayashi, H. Sawa, T. Takahashi, and T. Nakamura: J. Phys. Soc. Jpn. **76** (2007) 113702.
6) H. Sawa: private communication.
7) T. Kawai and A. Kawamoto: J. Phys. Soc. Jpn. **78** (2009) 074711.
8) R. Wojciechowski, K. Yamamoto, K. Yakushi, and A. Kawamoto: Synth. Met. **135–136** (2003) 587.
9) H. Seo: J. Phys. Soc. Jpn. **69** (2000) 805.
10) S. N. Magonov, G. Bar, H.-J. Cantov, J. Paradis, J. Ren, and M.-H. Whangbo: Synth. Met. **62** (1994) 83.
11) M. Yoshimura, H. Shigekawa, H. Yamochi, G. Saito, Y. Saito, and A. Kawazu: Phys. Rev. B **44** (1991) 1970.
12) M. Ishida, T. Mori, and H. Shigekawa: Phys. Rev. Lett. **83** (1999) 596.
13) M. Ishida, O. Takeuchi, T. Mori, and H. Shigekawa: Jpn. J. Appl. Phys. **39** (2000) 3823.
14) Y. Nogami and T. Mori: J. Phys. IV **12** (2002) Pr9-233.
15) N. Yoneyama, T. Sasaki, T. Nishizaki, A. M. Troyanovskiy, and N. Kobayashi: J. Low Temp. Phys. **142** (2006) 159.
16) H. Mori, S. Tanaka, and T. Mori: Phys. Rev. B **57** (1998) 12023.
17) K. Bender, I. Hennig, D. Schweitzer, K. Dietz, H. Endres, and H. J. Keller: Mol. Cryst. Liq. Cryst. **108** (1984) 359.
18) E. Clementi and D. L. Raimondi: J. Chem. Phys. **38** (1963) 2686.
19) J. Tersoff and D. R. Hamann: Phys. Rev. Lett. **50** (1983) 1998.
20) P. Guionneau, C. J. Kepert, G. Bravic, D. Chasseau, M. R. Truter, M. Kurmoo, and P. Day: Synth. Met. **86** (1997) 1973.